University of Baghdad
College of Engineering
JE
JOURNAL OF ENGINEERING

Journal of Engineering

journal homepage: www.jcoeng.edu.iq

Volume 32 Number 7 July 2026

Ultrasonically Synthesized Chitosan /PVA /PAA/Ag-Nanocomposites for Enhance Cement Mortar Performance

Zainab Taki Yonus *, Sana Hitur Awad

Department of Chemistry, College of Science for Women, University of Baghdad, Baghdad, Iraq

ABSTRACT

Yet little is known about the synergism of quaternary bio-based nanocomposite systems on cement mortar performance. For the first time, this research examines a quaternary nanocomposite comprising nano-chitosan, polyvinyl alcohol (PVA), polyacrylic acid (PAA), and silver nanoparticles (AgNPs) synthesized via ultrasonication and added to Ordinary Portland Cement mortar at 1.0 wt. % of cement. To study the effects of PVA and PAA on compressive strength, four systems (Za1–Za4) were fixed at nano-chitosan = 1.50 g and $AgNO_3$ = 10 mL while changing PVA content (0.25- 1.50 g) and PAA content (0.125-0.750 g) to a cement: sand ratio of 1:2.75 and w/c = 0.485. We compared these variables of compressive strength, water absorption, bulk density, and setting times. One-way ANOVA and Tukey's HSD confirmed that all the mixes were significantly different ($p < 0.001$). Results: The optimal mixture Za1 reported compressive strength 34.33 ± 0.058 MPa (4.7% increase), water absorption 2.77 ± 0.058% (31.7% reduction), bulk density of 2259 ± 1·0 kg/m^3, and setting time prolonged by initial and final, respectively, with values of 12.9% and 7·7%. In situ formation of AgNPs was confirmed by X-ray Diffraction (XRD), and Za1 exhibited a dense and homogeneous microstructure as revealed by Scanning Electron Microscopy (SEM) micrographs. C-S-H nucleation, pore-filling, crack-bridging, and nano-crosslinking mechanisms serve the process of improvement.

Keywords: Cement mortar, Nano-chitosan, Polyacrylic acid, Polyvinyl alcohol, Ultrasonic synthesis.

1. INTRODUCTION

Cement mortar made of cement is the basic support of contemporary construction because it has reasonable mechanical characteristics and economic viability. Nonetheless, over the last few years, there has been rising interest in improving its performance by integrating bio-based nanomaterial additives that contribute greatly to mechanical properties, resistance to environmental factors, and durability **(Abutu et al., 2025; Yang et al., 2025)**. Polymeric nanocomposites are regarded as one of the most notable advances in materials

*Corresponding author
Peer review under the responsibility of University of Baghdad.
https://doi.org/10.31026/j.eng.2026.07.04

Article received: 03/05/2026
Article revised: 09/06/2026
Article accepted: 09/06/2026
Article published: 01/07/2026

science, since they allow the combination of several properties into a single, coherent system, incorporating mechanical strength, thermal stability, and high surface activity, and providing a wide range of opportunities for use in engineering and construction **(Soman et al., 2023)**.

Chitosan has been widely modified and characterized using various spectroscopic and microscopic techniques, confirming its versatile chemical reactivity and functional group availability **(AL Sahib and Awad, 2022).** Nona-chitosan, in this regard, comes out as a promising biomaterial because of its unique physicochemical characteristics, such as biodegradability, non-toxicity, and the availability of active amino groups ($-NH_2$), which provide it with a positive charge that increases its interactions with nanoparticles and inorganic materials. Moreover, its large surface area at the nanoscale enhances dispersion and interfaces in the cement matrix, which has a positive effect on the microstructure and mechanical properties of cement mortar **(Saeed et al., 2024; Gonzalez-Lara et al.,2025).** Novel chitosan-dependent Schiff bases were synthesized and characterized by the reaction of chitosan with para-hydroxybenzaldehyde and malic anhydride, resulting in the formation of functional derivatives associated with diverse amino and hydroxyl aggregates. The results of spectroscopic analyses using FT-IR and $H\text{-}NMR^1$ confirmed the successful conversion of the chitosan amine (NH_2) groups to amine bonds (C=N), demonstrating the high reactivity of the chitosan functional aggregates and their susceptibility to additional chemical modifications. The prepared derivatives have also shown significant antimicrobial activity, reinforcing the importance of chemically modified chitosan as a multifunctional substance with promising bio applications **(AL-Sahib et al., 2022)**. These properties have also led to the use of nano-chitosan in the construction and cementitious materials industry **(Baykara et al., 2024)**, where it promotes the development of calcium silicate hydrate (C–S–H) gel in two ways. First, a physical effect that involves the filling of micropores and densification of the interfacial transition zone (ITZ) between cement paste and aggregates, leading to a decrease in porosity and an increase in bulk density.

The other is a chemical effect, in which nano-chitosan provides nucleation sites for hydration reactions and the formation of C-S-H gel to improve the compressive strength of cementitious materials by 10% to 15% with an optimum content **(Pan et al., 2024)**. Polyvinyl alcohol (PVA) is a commonly used water-soluble synthetic polymer in new advanced materials because of the presence of hydroxyl groups (OH), which give it a strong hydrogen -bonding capability with other polymer chains **(Alwan and Kadhim, 2025; Fang et al.,2024)**. PVA helps to improve water resistance in cement mortar by filling capillary pores and lowering permeability since its chains form a hydrophilic network that prevents water flow and increases cohesion **(Choi et al., 2021)**. Conversely, polyacrylic acid (PAA) contains ionic groups of carboxylic acid (-COOH), which form complexes with free calcium ions in cement, delaying the initial setting time, a positive effect in casting for enhancing workability **(Yehia et al., 2023; Yu et al.,2025)**. This property also allows for the formation of the so-called dense Three-dimensional interconnected polymer networks with nano-chitosan and PVA via hydrogen bonding and electrostatic interactions **(Abdali et al., 2023)**. These networks have been proven to improve the mechanical and optical characteristics of the polymer systems **(Al-Fawares et al., 2024)**. Silver nanoparticles (AgNPs), derived from silver nitrate ($AgNO_3$), confer enhanced functional features to the composite, such as antimicrobial behavior, thermal and electrical conductivity, as well as the formation of nano-crosslinking points in the polymer matrix, improving the mechanical properties and resistance to deformation **(Abdul Kareem et al., 2023; Chicea and Nicolae-Maranciuc,**

2024; Paciejewski et al., 2024). The incorporation of AgNPs in cementitious systems has been shown to significantly reduce microbial growth while simultaneously enhancing cement mortar durability in aggressive environments **(Sybis, 2026).** The size and distribution of the nanoparticles are influenced by various factors, including the concentration of ions, the type of reducing agent used, and the role of polymers as stabilizers **(Han et al., 2023)**. Ultrasonication has been of significant interest as a method of preparing nanocomposites because of the acoustic cavitation phenomenon, whereby microbubbles are formed and collapse violently, producing a localized high pressure and temperature **(Suslick and Price, 2010)**. This action results in deagglomeration of nanoparticles, even dispersion, and increased interfacial interactions between composite components **(Soman et al., 2023).** Research has shown that ultrasonication enhances rheological and mechanical properties to a greater level than traditional mixing methods **(Popescu et al., 2022)**.

There are many studies of binary and ternary polymer nanocomposite systems on the properties of cement mortar, but with regard to the synergistic effect, research in quaternary hybrid nanocomposite systems also has a large gap in the literature. Most of the previous studies were devoted to binary -based combinations such as chitosan/PVA **(Saeed et al., 2024),** chitosan/AgNPs **(Chicea and Nicolae-Maranciuc, 2024)** or PVA/AgNPs **(Aldakheel et al., 2023),** whereas only a few investigations dealt with ternary systems **(Mohamed, 2022; Popescu et al., 2022)**. However, to the best of the authors' knowledge, it is indeed unclear which previous study has been performed simultaneously both in combination (nano-chitosan as well as PVA or PAA and AgNPs) synthesized via ultrasonication, and to combine all components into a quaternary nanocomposite system subsequently blended with Ordinary Portland Cement mortar by varying weight ratios. Additionally, the distinct role of PAA as a fourth component in controlling setting time and strengthening the three-dimensional polymer network inside the cement matrix, together with the in situ creation of AgNPs from $AgNO_3$ under ultrasonication conditions, is a novel approach that has not been reported to date. Hence, this research aims to fill this gap in the literature by systematically evaluating the influence of PVA and PAA concentrations in a multicomponent nanoscale system on several mechanical and physical properties of normal bonded mortar vital for most construction-related applications, by preparing these samples as per **(ASTM C109, 2021)** guidelines. The significance of examining the quaternary nanocomposites made of nano-chitosan, PVA, PAA, and silver nanoparticles prepared at varying ratios through ultrasonication lies in the fact that the relationship between chemical structure, microstructure, and functional properties **(Mohamed, 2022)** must be explored, and thus optimal composition which denotes a balance between physical, mechanical and chemical properties **(Aldakheel et al., 2023)** must be obtained. Literature suggests that these systems are thorough in their improvement, such as improving compressive strength, minimizing water absorption, setting time, and increasing bulk density, and have potential as additives to high-technology building materials with engineering and environmental advantages **(Abutu et al., 2025; Yang et al., 2023; Yang et al., 2025).**

Thus, this research aims to be the first systematic study examining a quaternary hybrid nanocomposite system of nano-chitosan, PVA, PAA and AgNPs prepared by ultrasonication at a fixed nano-chitosan weight: $AgNO_3$ volume ratio but variable PVA and PAA concentrations on compressive strength, water absorption, bulk density and setting times of regular OPC mortar based on ASTM C109. Differing from previous research where binary or ternary polymer nanocomposite systems were employed, this study couples four functional components in a single ultrasonication-assisted synthesis process and takes advantage of

the synergistic interactions of nano-chitosan nucleation effect, PVA and PAA pore-filling and crack-bridging roles, as well as AgNPs nano-crosslinking effect in cement mortar to yield unique mechanical and physical enhancement.

2. MATERIALS AND METHODS

2.1 Materials

2.1.1 Cement

The Ordinary Portland Cement (OPC) used in this study was produced by the Tsluja Cement factory in all cement mortar mixtures and conformed to the requirements of the Iraqi Specification **(IQS No. 5, 2019)**, Type 42.5N. **Tables 1 and 2** present the chemical and physical parameters of this cement, respectively

Table 1. Cement's Chemical Composition and Main component

Oxide composition	Test results%	(IQS No. 5, 2019) requirements
CaO%	63.2	--
Fe_2O_3%	3.5	--
Al_2O_3%	5.1	--
SiO_2%	20.85	--
MgO%	2.1	≤5.0%
SO_3%	2.2	--
Loss on Ignition %	2.14	≤4.0%
Insoluble residue	0.9	≤1.5
Main Compounds of Cement		
Tri-Calcium Silicate (C_3S) %	55.0	
Di-Calcium Silicate (C_2S) %	18.2	
Tri-Calcium Aluminate(C_3A) %	7.6	
Tetra-Calcium-AluminateFerrite (C_3AF %	107	

Table 2. Cement's Physical Properties

Properties	Results	(IQS No. 5, 2019) requirements
Soundness(mm)-(Autoclave)%	1.5	≤10mm
Setting Time (Vicat's)		
Initial(min)	134 min	≥45min
Final(hr.)	4.5hr.	≤10hr
Fineness-Blaine (m^2/Kg)	350	≥250
Compressive Strength (MPa)		
At 2-days	25	10≤
At 28-days	49	42.5≤

2.1.2 Standard Sand (S.S)

In the current tests for cement mortar, standard sand was used for the preparation of the cement mortar samples obtained from the General Company for Mining Industries, one of the formations of the Ministry of Industry and Minerals. This sand, also known as silica sand, is naturally made primarily of quartz and is distinguished by its purity and by the grains that

retain their natural shape, as shown in **Fig. 1.** The grading of the standard sand used in this research was (20-30) and met the requirements of ASTM C778 specifications. It consisted of about 92% silica. The sieve analysis results of the standard sand (SS) and the limits given by ASTM C778 are shown in **Table 3**. The results of the grading were within the specification limits.

Figure 1. Standard sand**.**

Table 3. Gradation of standard sand and values of limits

Sieve size		Passing (%)	Requirements gradation (ASTM C778, 2017)
in	mm		
No.16	**1.18**	100	100
No.20	**0.850**	90.2	85-100
No.30	**0.600**	2.5	0-5

2.1.3 Water

The water used in this study for mixing is sourced from the drinking water supply of Baghdad city and also for curing purposes, and complies with **(IQS No. 1703, 2018).**

2.1.4 Chemical materials

Nano-chitosan with particle size less than 100nm and degree of deacetylation ≥85% was supplied by Nanochemazon Co., Canada. Polyvinyl alcohol (PVA), polyacrylic acid (PAA), and glycial acetic acid were obtained from Fluka Chemika, Germany. Silver nitrate ($AgNO_3$) purity≥99.9%was purchased from BDH Laboratory Supplies, UK.

2.2 Preparation

2.2.1 Preparation of Hybrid Composite

The respective components were prepared independently before the synthesis of the nanocomposites. The prepared nano-chitosan was dissolved in glacial acetic acid; 10 mL of glacial acetic acid was added dropwise to the assigned weight of nano-chitosan at room temperature and stirred continuously for 10–15 minutes until a uniform solution was obtained. A sufficient amount of polyvinyl alcohol (PVA) was added and dissolved with continuous stirring for 10-15 minutes in distilled water at a temperature of 60–75°C until all PVA went into solution. Polyacrylic acid (PAA) was used as received without pre-dissolution. Quaternary nanocomposites were subsequently prepared using a stainless steel ultrasonic bath (frequency: 20 kHz, maximal power: 400 W). In each nanocomposite, the prepared nano-chitosan solution was mixed with PVA solution, and then the particular weight of PAA (as mentioned in **Table 4**) and 10 mL $AgNO_3$ solution were added according to the mixing proportions **Table 4.** This blended mixture in the ultrasonic bath was then ultrasonicated by applying a temperature of 70°C for 90 minutes under maximum power. Ultrasonication generated acoustic cavitation, which stimulated the in situ reduction of Ag^+ ions to form

AgNPs embedded into the polymer matrix due to amino groups (-NH_2) present within nano-chitosan (NC-Ag). At the same time, due to the ultra-high energy of cavitation, all components were evenly dispersed, while molecular-level interactions via hydrogen bonds and electrostatic interactions between nano-chitosan and PVA/PAA chains were achieved, forming an efficient cross-linked structure **(Soman et al., 2023; Suslick and Price, 2010).** The nanocomposites obtained in this way were quenched to room temperature before use.

Table 4. The ratios of the composites

Sym. of Specimens	Chitosan(gm)	PVA (gm)	PAA (gm)	$AgNO_3$(mL)(250mg/L)
Za1	1.5	1.5	0.75	10
Za2	1.5	1.0	0.5	10
Za3	1.5	0.5	0.25	10
Za4	1.5	0.25	0.125	10

2.2.2 Preparation of Mortar

The cement mortar specimens were cast according to ASTM C109. The standard cement mortar was made with a weight ratio of 1:2.75 cement to standard sand. The water-cement ratio was kept at 0.485 for all the mixes containing Portland cement. The specimens were cast in stainless steel cube molds measuring (5 × 5 × 5) cm (50 × 50 × 50) mm; see **Fig. 2**. **Table 5** shows the amount of each material used for preparing a mortar batch to cast six, nine and twelve specimens.

Table 5. The quantity of materials for preparing a mortar.

No. of Specimens	6	9	12
Cement (gm)	500	740	1060
Standard sand(gm)	1375	2035	2915
Water (mL)	242	359	514

Figure 2. Specimens of mortar

2.2.3 Mix Design

The control mix (M0) consisted of ordinary Portland cement and standard sand without any additives, prepared in accordance with **(ASTM C109, 2021)** with a water-to-cement ratio of 0.485. Four additional mixes (Za1–Za4) were prepared by incorporating the quaternary nanocomposites in dry powder form at a dosage of 1% by dry weight of cement. The nanocomposite powder was manually blended with the dry cement prior to water addition using a 500ml ceramic crucible with a ceramic stirring rod until a visually homogeneous mixture was achieved, ensuring uniform distribution of the nanocomposite within the cement powder before water addition. The water-to-cement ratio was maintained at 0.485

for all mixes, and no adjustment was made to the mix water content. Three 50×50×50 mm cubic specimens were cast for each mix, resulting in a total of fifteen specimens.

2.3 Tests Conducted

2.3.1 Compressive Strength

The compressive strength of cement mortar specimens was measured after 7 and 28 days of curing according to **(ASTM C109, 2021).** Three cubes (50×50×50 mm) for each mix were cast and cured in water at room temperature (23±2°C). The compressive strength was determined as an average of three specimens for each mix. The compressive strength was determined with Eq. (1):

$$f'c = P / A \quad (1)$$

With f'c being the compressive strength (MPa), P the maximum load (N) and A the cross-sectional area (mm^2).

2.3.2 Water Absorption and Hardened Mortar Bulk Density

Both water absorption and hardened mortar Bulk Density were determined after 28 days of curing in accordance with **(ASTM C642, 2021)**. Specimens were oven-dried at 105±5°C for 24 hours and weighed in air (A). Specimens were then immersed in water at room temperature for 24 hours, weighed while suspended in water (C), and weighed again in air after surface drying (B). Water absorption and bulk density were calculated using the following Eqs. (2) and (3), respectively:

$$WA (\%) = [(B - A) / A] \times 100 \quad (2)$$

$$\rho = [B / (B - C)] \times \rho w \quad (3)$$

Where:

WA = water absorption (%)
ρ = Bulk Density of hardened mortar (kg/m^3)
A = mass of oven-dried specimen in air (g)
B = mass of surface-dry specimen in air after immersion (g)
C = apparent mass of specimen suspended in water (g)
ρw = bulk density of water (1000 kg/m^3)

2.3.3 Initial and Final Setting Time

The setting time of cement paste was measured using the Vicat apparatus as per **(ASTM C191/C191M, 2021).** The standard consistencies of the cement mixes were determined before the setting time test. The nanomaterial additives were added to the mixing water at 1% by weight of cement before testing. Setting times were recorded as follows:
Initial Setting Time: Time from water addition until the Vicat needle failed to penetrate to within 25 mm of the bottom of the mold.
Final Setting Time: The time elapsed from water addition until the Vicat needle failed to leave any mark on the cement paste. The tests were performed at a room temperature of 23±2°C and a relative humidity of 50±5 %.

2.3.4 Characterization of Nanocomposites

The synthesized nanocomposites were characterized using X-ray diffraction (XRD) and scanning electron microscopy (SEM). XRD analysis was performed using an X-ray diffractometer with CuKα radiation (λ = 1.5406 Å) at a scanning rate of [X]°/min over a 2θ range of 10°–80°. SEM analysis was conducted at NanoLAB-MOST using an accelerating voltage of 20.0 KV.

3. RESULTS AND DISCUSSION

The results of all conducted tests are summarized in **Table 6.** One-way ANOVA followed by Tukey's HSD post-hoc test was performed to evaluate the statistical significance of differences between mixes. All results are presented as mean ± standard deviation (SD) of three replicates. A p-value less than 0.05 was considered statistically significant in **Tables 7 to 10.**

Table 6. Mechanical and Physical properties of cement mortar mix

Sym. of mix	Compressive Strength(7day) MPa	Compressive Strength(28day) MPa	Water Absorption (%)	Bulk density (Kg/m²)	Initial setting time(min)	Final setting time(min)
control	26.9	32.80	4.2	2236	171	285
Za1	28.2	34.33	2.77	2259	193	307
Za2	27.16	33.73	3.1	2254	190	301
Za3	27.24	33.50	3.5	2248	185	295
Za4	26.5	33.23	3.6	2245	180	290

Table 7. Statistical Summary of All Test Results (Mean ± SD)

Mix	CS 7-day (MPa)	CS 28-day (MPa)	WA (%)	Bulk density (kg/m³)
MO	26.90 ± 0.100	32.80±0.1	4.2±0.1	2236±2.0
Za1	28.20 ± 0.100	34.33±0.058	2.77±0.058	2259±1.0
Za2	27.17±0.058	33.73±0.058	3.1±0.1	2254±4.0
Za3	27.23±0.115	33.5±0.1	3.5±0.1	2248±5.6
Za4	26.5±0.1	33.23±0.058	3.6±0.2	2245±4.4

Table 8. Summary of one-way ANOVA statistical analysis for compressive strength, water absorption, bulk density of cement mortar mixes incorporating quaternary nanocomposites

Property	F-Value	P-Value	Significance
CS-7days	127.14	<0.001	***
CS-28days	163.5	<0.001	***
Water Absorption	60.11	<0.001	***
Bullk density	16.33	<0.001	***

Note: *** indicates highly significant difference at $p < 0.001$

3.1 Compressive Strength

The compressive strengths of cement mortar mixes at 7 and 28 days of curing are shown in **Table 6 and Fig. 3(a, b)**. One-way ANOVA revealed highly significant differences among all mixes at both ages ($F = 127.14$, $p < 0.001$ at 7 days; $F = 163.50$, $p < 0.001$ at 28 days), and Tukey's HSD post-hoc test confirmed that nearly all pairwise comparisons were statistically significant ($p < 0.05$), except Za2 vs Za3 at 7 days, which showed no significant difference ($p > 0.05$) as shown in **Tables 8 and 9**

Table 9. Tukey's HSD post-hoc test results for compressive strength at 7 and 28 days

Comparison	Diff 7-day (MPa)	Significance	Diff 28-day (MPa)	Significance
MO vs Za1	1.3	Yes*	1.533	Yes*
MO vs Za2	0.267	Yes*	0.933	Yes*
MO vs Za3	0.333	Yes*	0.700	Yes*
MO vs Za4	0.4	Yes*	0.433	Yes*
Za1 vs Za2	1.033	Yes*	0.600	Yes*
Za1 vs Za3	0.967	Yes*	0.833	Yes*
Za1 vs Za4	1.700	Yes*	1.100	Yes*
Za2 vs Za3	0.067	No	0.233	Yes*
Za2 vs Za4	0.667	Yes*	0.500	Yes*
Za3 vs Za4	0.733	Yes*	0.267	Yes*

Note: * indicates significant difference at $p < 0.05$; No indicates no significant difference ($p > 0.05$)

The results demonstrate that the incorporation of quaternary nanocomposite additives at 1% by weight of cement led to a progressive improvement in compressive strength with increasing nanocomposite concentration. At 7 days, mix Za1 recorded the highest compressive strength of 28.20 ± 0.100 MPa compared to 26.90 ± 0.100 MPa for the control mix (M0), representing a statistically significant improvement of 4.8%. At 28 days, Za1 maintained its superiority with a compressive strength of 34.33 ± 0.058 MPa, corresponding to a 4.7% increase over the control mix (32.770 ± 0.100 MPa). This behavior is consistent with previous findings on nano-pozzolanic materials incorporated into cement mortar, which demonstrated significant improvements in microstructure and mechanical performance through pore refinement and densification of the cement matrix **(Rasin et al., 2017).** The strength enhancement observed in Za1 is attributed to the synergistic effect of its constituents at higher concentrations, operating through three distinct mechanisms. The first mechanism is the pore-filling effect**,** whereby nano-chitosan particles, owing to their nanoscale dimensions and high surface area, effectively fill the capillary pores and micro-voids within the cement matrix, reducing porosity and increasing the bulk density of the hardened paste **(Baykara et al., 2024)**. This physical densification directly contributes to the observed increase in compressive strength by reducing stress concentration points within the matrix. The second mechanism involves C-S-H gel formation enhancement, in which nano-chitosan acts as a nucleation agent, providing additional nucleation sites that accelerate the hydration reactions and promote the formation of a denser and more uniform calcium silicate hydrate (C-S-H) gel network **(Pan et al., 2024).** The densification of the interfacial transition zone (ITZ) between cement paste and aggregate represents a particularly significant contribution, as the ITZ is typically the weakest region in cementitious composites and its strengthening has a disproportionately large effect on overall compressive strength. The third mechanism is the polymer network formation, in which the higher concentrations of PVA (1.50 g) and PAA (0.75 g) in Za1 promote the formation of a dense three-dimensional cross-linked polymer network through extensive hydrogen bonding between the hydroxyl groups (-OH) of PVA and the carboxylic groups (-COOH) of PAA, as well as electrostatic interactions with the amino groups ($-NH_2$) of nano-chitosan **(Choi et al., 2021)**. This interconnected polymer network bridges micro-cracks within the cement matrix, effectively restricting crack propagation under compressive loading and contributing to the observed strength gain. Furthermore, the AgNPs generated in-situ from $AgNO_3$ under ultrasonication conditions provide additional nano-crosslinking points within the polymer network, reinforcing the matrix at the nanoscale level and filling residual micro-voids that contribute to strength improvement **(Abdul Kareem et al., 2023;**

Paciejewski et al., 2024). With decreasing nanocomposite concentration from Za2 to Za4, compressive strength values declined progressively, recording 28-day values of 33.73 ± 0.058, 33.50 ± 0.100, and 33.23 ± 0.058 MPa, respectively. Despite this reduction, all nanocomposite mixes surpassed the control mix at both testing ages, confirming the beneficial role of the quaternary nanocomposite system across all tested concentrations. The progressive decline in strength with decreasing concentration is attributed to the reduced availability of polymer chains and nanoparticles for pore filling, C-S-H nucleation, and network formation at lower dosages **(González-Lara et al., 2025)**. It is noteworthy that Za2 and Za3 showed no statistically significant difference in 7-day compressive strength (Tukey's HSD, $p > 0.05$), suggesting that beyond a certain threshold concentration, the marginal contribution of additional polymer content to early-age strength becomes negligible, while the 28-day results showed significant differences between all mixes, indicating that the long-term hydration process amplifies the differences in microstructural development induced by varying nanocomposite concentrations.

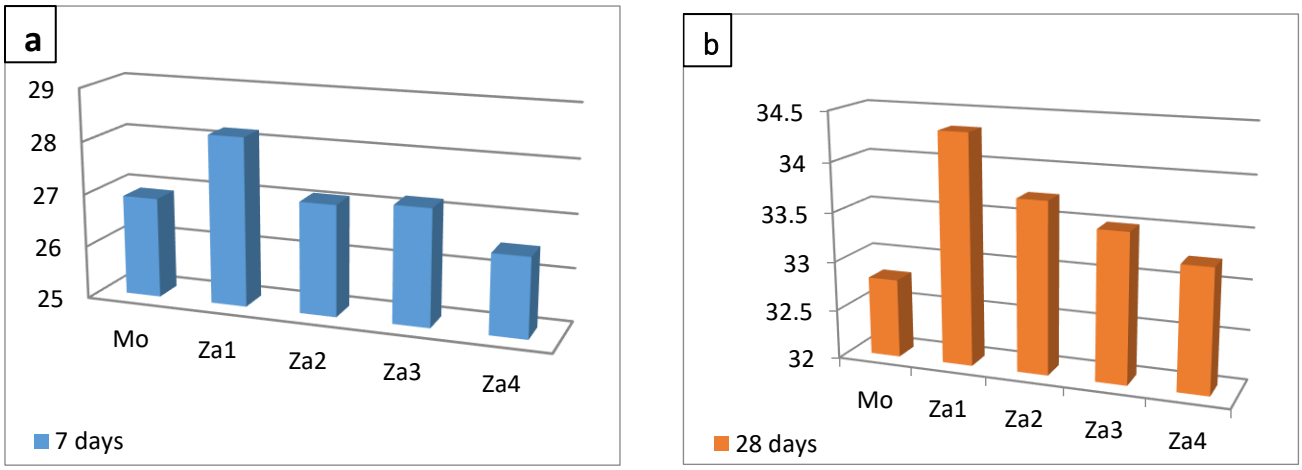

Figure 3. (a) Compressive strength at 7 days (MPa), **(b)**Compressive strength at 28 days (MPa)

3.1 Water Absorption and Hardened Mortar Bulk Density

Table 10. Tukey's HSD post-hoc test results for water absorption and hardened mortar bulk density

Comparison	Diff WA%	Sig.	Diff Bulk density (Kg/m³)	Significance
MO vs Za1	1.433	Yes*	23.000	Yes*
MO vs Za2	1.100	Yes*	18.000	Yes*
MO vs Za3	0.700	Yes*	12.000	Yes*
MO vs Za4	0.600	Yes*	9.000	No
Za1 vs Za2	0.333	Yes*	5.000	No
Za1 vs Za3	0.733	Yes*	11.000	Yes*
Za1 vs Za4	0.833	Yes*	14.000	Yes*
Za2 vs Za3	0.400	Yes*	6.000	No
Za2 vs Za4	0.500	Yes*	9.000	No
Za3 vs Za4	0.100	No	3.000	No

Results for the water absorption and hardened mortar bulk density after 28 days of curing are presented in **Table 6 and Fig. 4(a, b)**. The findings show a steady and progressive improvement in both of the parameters with increasing concentrations of the

nanocomposite, with Za1 showing the highest durability among all the mixes. The lowest water absorption was found in Za1, with 2.77%, which is 31.7% lower than the control mix (4.1%). This remarkable reduction is due to the pore-filling action of the increased nano-chitosan, PVA, PAA and AgNPs present in Za1. The nano-chitosan particles, with their large surface area and positive surface charge, filled the capillary pores of the cement matrix and increased the particle packing of the ITZ **(Baykara et al.,2024)**. The increased PVA content (1.50 g) formed a continuous hydrophilic network, which connected micro-cracks and decreased the connectivity of capillary pores, and the higher PAA concentration (0.75 g) reacted with free calcium ions to form extra hydration products that further tightened the paste structure **(Mohamed, 2022)**. The AgNPs formed in-situ within the polymer matrix under the influence of ultrasonication also resulted in additional nanopore filling, thereby preventing water movement through the hardened cement mortar **(Aldakheel et al.,2023).** Studies have indicated the existence of **s**imilar mechanisms for filling spaces and pores in polymer-based hybrid nanosystems added to cement mortar, where the cohesive polymeric lattice structure significantly reduced the rate of water absorption, as well as enhancing the permeability resistance of the cement matrix and improving its structural cohesion **(Watanuki Filho et al., 2022).** As a result, Za1 had the highest mortar bulk density in the hardened state (2259 kg/m^3) compared to 2236 kg/m^3 for the control mix, which represents an increase of 23 kg/m^3. The inverse trend between water absorption and bulk density across all mixes validates the physical soundness of the results, as the denser the matrix, the less porous it is and the lower the water absorption **(Suarez abd Rincon,2025)**. Increasing water absorption (from 3.1% to 3.6%) and decreasing bulk density (from 2254 to 2245 kg/m^3) as the nanocomposite concentration decreased from Za2 to Za4 further support the validity of the experimental results. This gradient behavior also confirms the dose-dependent nature of the quaternary nanocomposite and is in agreement with the findings of **(Popescu et al., 2022)**, who reported a denser cement matrix and lower water absorption as the concentration of PVA/chitosan/AgNPs nanocomposites increased.

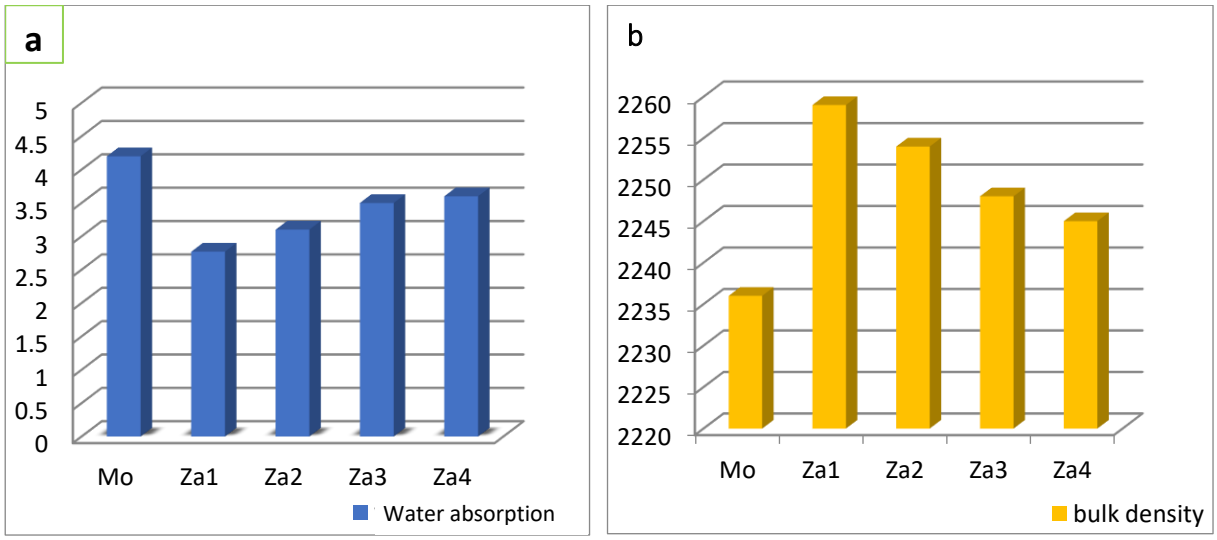

Figure 4. (a) Water Absorption % and (b) Hardened mortar bulk density (kg/m^3)

The observed reduction and the corresponding increase in bulk density indicate that the quaternary nanocomposite contributed to pore refinement and matrix densification, thereby restricting water ingress into the cement mortar. These findings suggest an improvement in the resistance of the modified mortar to moisture transport. Although

contact angle measurements were not conducted in the present study, such analysis could prove addition information regarding surface wettability and hydrophobicity and would be valuable for further verification of the water transport behavior of the developed nanocomposite modified mortar

3.2 Initial and Final Setting Time

The initial and final setting times of different mixes are shown in **Table 6, Fig. 5**. The setting times of all the nanocomposite mixes were greater than the control mix (M0: IST = 171 min, FST = 285 min), thereby confirming the retardation of cement hydration caused by the quaternary nanocomposite additives. This effect became more pronounced as the concentration of nanocomposite increased, with Za1 showing the longest initial and final setting times of 193 and 307 minutes, respectively. This phenomenon in Za1 corresponds to a 12.9% and 7.7% increase in the initial and final setting times, respectively, compared to the control mix. This is mainly due to the increased concentration of PAA (0.75 g) in Za1, which interacts with free calcium ions (Ca^{2+}) in cement paste to form calcium polyacrylate complexes that temporarily coat cement particles and prevent the commencement of hydration reactions **(AL-Fawares et al., 2024)**. This retarding behavior is in good agreement with **(Yu et al., 2025),** who demonstrated that PAA and PVA polymer binders reduce early –age strength while extending setting times in cement-based systems through adsorption on cement particle surfaces. The increased PVA concentration (1.50 g) also played a role in delaying setting times, with adsorption of its hydroxyl groups (-OH) onto cement particles forming a thin layer on their surfaces, temporarily preventing water penetration into unhydrated clinker phases **(Yehia et al., 2023).** Ultrasonication ensured homogeneous dispersion of both PVA and PAA molecules across the cement paste, allowing them to interact fully with cement particles and impart maximum retardation effect **(Soman et al., 2023).** As the nanocomposite content was reduced from Za2 to Za4, initial and final setting times gradually decreased, with values of 190, 185 and 180 minutes for IST and 301, 295 and 290 minutes for FST, respectively. Yet, all mixes showed setting times that were significantly longer than the control mix and still within acceptable limits for field applications as stipulated by **(ASTM C191/C191M, 2021)**. It's worth noting that the longer setting times observed for all the nanocomposite mixes present a great practical benefit to construction work in hot climatic zones, like that in Iraq, where increased workability is highly desirable to aid in cement mortar placement and compaction in the field **(Choi et al., 2021)**.

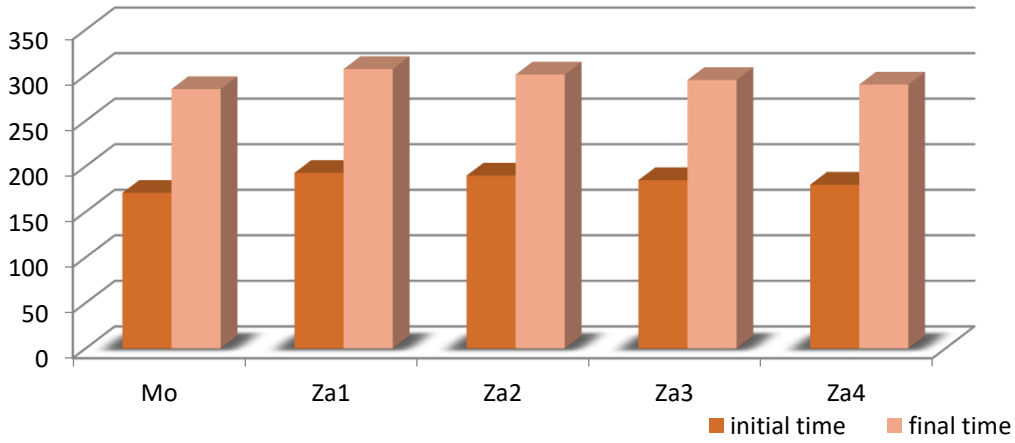

Figure 5. Initial and final setting time (min)

3.4 XRD Analysis

The XRD patterns of nanocomposites Za1 and Za3 are presented in **Fig. 6(a, b),** respectively. Both patterns were recorded over a 2θ range of 10°–80° using CuKα radiation (λ = 1.5406 Å).

Both nanocomposites exhibit a broad amorphous hump centered at approximately 2θ ≈ 20°, confirming the predominantly amorphous character of the quaternary polymer matrix. This broad peak is characteristic of semi-crystalline PVA and indicates that the ultrasonication process successfully promoted molecular-level interactions between nano-chitosan, PVA, PAA, and AgNPs, disrupting the individual crystalline structures of the components and producing a homogeneous nanocomposite system **(Soman et al., 2023)**.

A notable difference between the two patterns is the diffraction intensity, where Za3 exhibited a significantly higher peak intensity (~370 counts) compared to Za1 (~140 counts). This is attributed to the higher degree of polymer chain entanglement and cross-linking in Za1 due to its greater PVA and PAA concentrations, which further reduced the crystalline order of the matrix and produced a more amorphous structure **(Abdali et al., 2023)**.

Notably, no distinct diffraction peaks corresponding to crystalline AgNPs were detected at the expected positions of 2θ = 38.1°, 44.3°, and 64.4°, confirming that AgNPs were successfully incorporated at an extremely fine nanoscale level within the polymer matrix with superior dispersion achieved through ultrasonication **(Chicea and Nicolae-Maranciuc, 2024).**

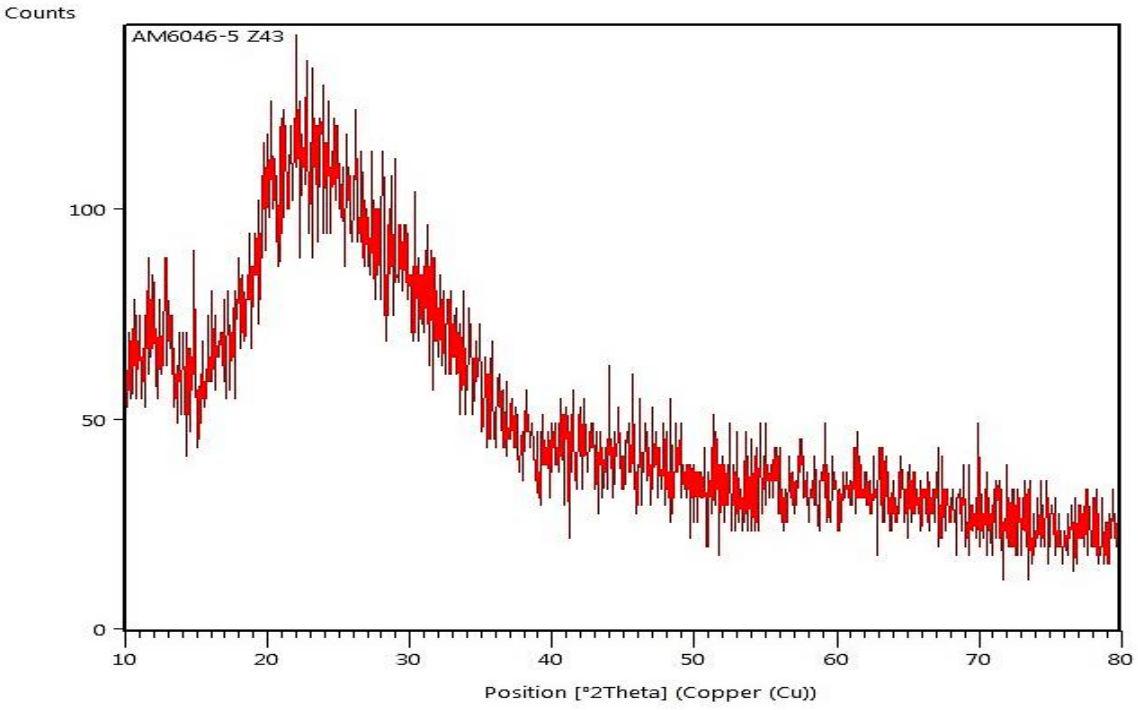

(a)

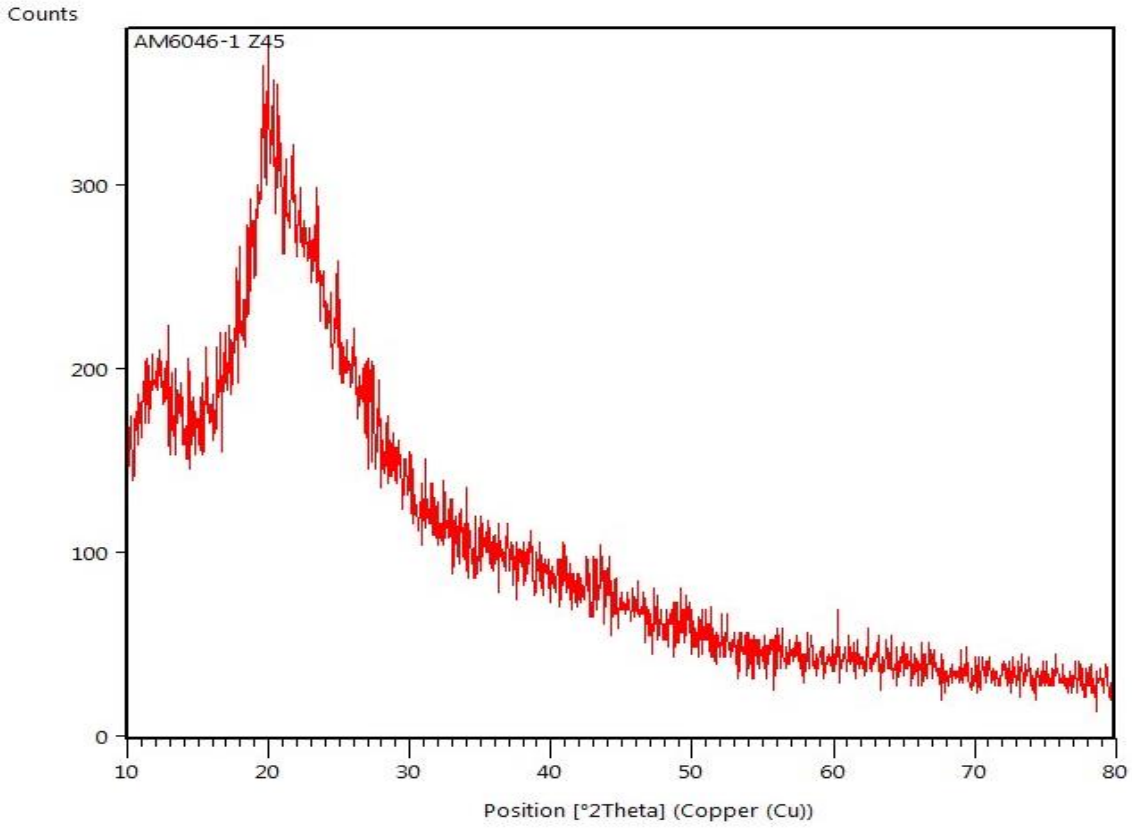

(b)

Figure 6. (a) XRD analysis of Za1(Z43)* and **(b).** XRD analysis of Za3(Z45)*

3.5 SEM Analysis

The micrographs of Za1 nanocomposite (highest concentrations of PVA (1.50 g) and PAA (0.75 g) are shown in **Fig.7 (a–d)** at magnifications of 10.00 kx, 5.00 kx, and 1.00 kx and 200x, respectively.

The microstructure of Za1 is dense, smooth, homogeneous and crack-free with no visible macro-pores, inter-phase boundaries or particle agglomerates for all such magnification levels. At the highest magnification (**Fig. 7a**,10.00 kx, scale bar = 5 µm), fine undulating lines depicting the entangled three-dimensional polymer chain network are distinctly observed, attesting to extensive intermolecular hydrogen bonding and electrostatic interactions between nano-chitosan, PVA and PAA chains **(Saeed et al., 2024)**. At (**Fig. 7b**, 5.00 kx , scale bar=10µm), the dispersed nano-scale bright particles in uniform distribution demonstrate the successful in-situ formation and homogenous dispersion of AgNP into the polymer matrix in submicron under ultrasonication conditions **(Abdul Kareem et al.,2023)**. At intermediate magnification, (**Fig. 7c,** 1.00 kx, scale bar = 50 µm) shows a spherical single particle approximately equal to 5–8 µm and with a smooth interface indicating strong interfacial adhesion regarding nanocomposite constituents **(AL-Fawares et al., 2024)**. At the lowest magnification (**Fig. 7d**, 200×, scale bar = 200 µm), the entire field of view appears homogenized and featureless at the surface, indicating macro-scale homogeneity and again validating ultrasonication as preventing phase separation **(Soman et al., 2023)**.

The excellent mechanical and physical behavior of Za1, namely the highest 28-day compressive strength (34.33 ± 0.058 MPa), lowest water absorption (2.77 ± 0.058%),

highest bulk density (2259 ± 1.0 kg/m3) as well as longest setting times (IST =193 min, FST=307 min) among all tested mixes is directly attributable to its dense and homogeneous microstructure confirmed statistically significant by Tukey's HSD test at $p < 0.05$ level **(Baykara et al., 2024; Abutu et al., 2025).**

Fig. 8(a–d, at 10.00 kx, 5.00 kx, 1.00 kx and 200× magnification, respectively) shows SEM micrographs for Za3 nanocomposite at lower concentrations of PVA (0.50 g) and PAA (0.25 g). Unlike Za1, which has a relatively smooth morphology at all magnifications, Figure 7(a-d) shows that Za3 possesses a rough lamellar porous microstructure with visible inter-lm voids and fractured plate-like features. At the highest magnification **(Fig. 8a,**10.00 kx, scale bar = 5 μm). In contrast, large plate-like lamellar structures separated by inter-crystalline voids were clearly resolved, which reflects a lower degree of polymer chain entanglement as a result of the lower PVA and PAA concentrations **(Abdali et al., 2023).** At 5.00 kx (**Fig. 8 b,** scale bar = 10 μm), several agglomerates of nano-chitosan are observed in the upper area, which suggested that lower dosages of polymers were unable to properly stabilize nanoparticles **(AL-Fawares et al., 2024).** At intermediate magnification **(Fig. 8c,** 1.00 kx, scale bar as well = 50 μm). The layered and porous nature of the matrix is further displayed by indicating less intermolecular attractions originating from nanocomposite components. At the lowest magnification **(Fig. 8d**, 200×, scale bar = 200 μm), large fragmented regions corroborate macro-scale phase heterogeneity due to inadequate polymer encapsulation from ultrasonication

The nature of the Za3 microstructure, which is more porous and heterogeneous than that of Za1, clearly matches its lower mechanical and physical performance at 28 days, with respect to compression strength (33.50 ± 0.100 MPa vs. 34.33 ± 0.058 MPa) [Tukey's HSD test ($p < 0.05$)], water absorption (3.50 ± 0.100% vs.2.77±0.058% lower bulk density (2248±5.6 vs 2259±1.0Kg/m^3), and shorter setting time (IST=185 VS 193 min), all difference confirmed as statistically significant by Tukey's HSD test ($p<0.05$) level **(Baykara et al., 2024; Suarez and Rincon, 2025).**

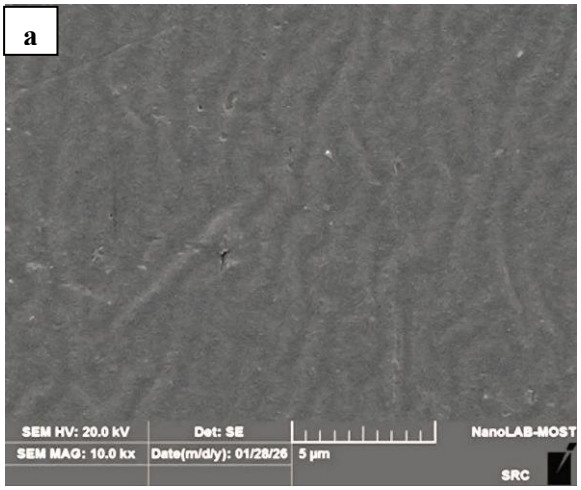

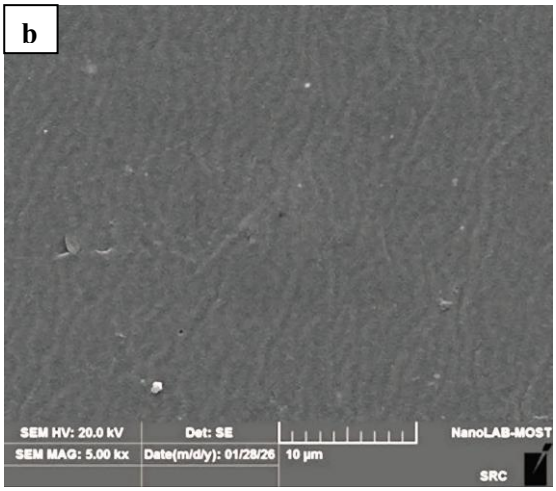

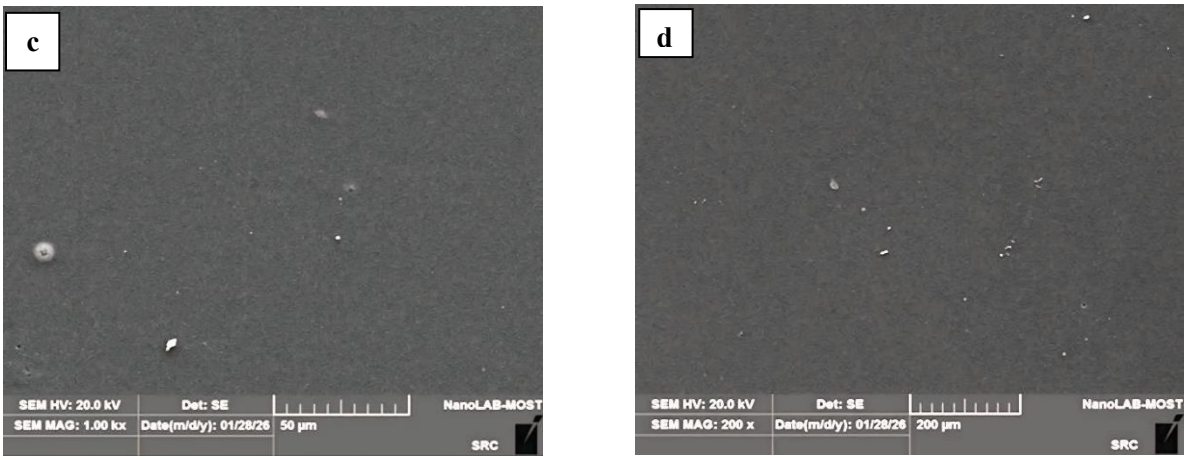

Figure 7. The SEM micrographs of Za1(Z43)* at different scales

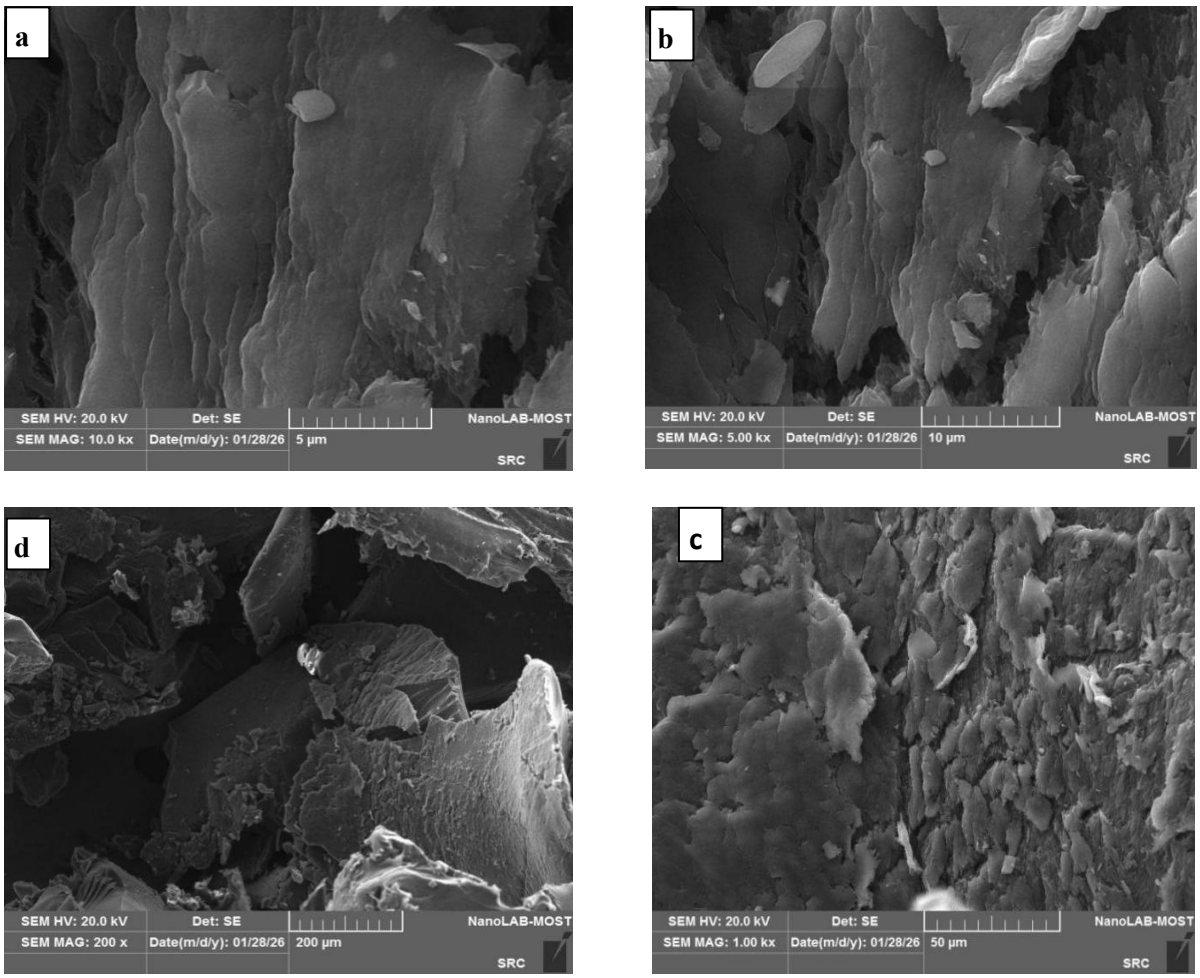

*The sample codes used by the XRD instrument (Z43, Z45) correspond to the mix designations used in this study (Za1,Za3).

Figure 8. The SEM micrographs of Za3(Z45)* at different scales

The steady decrease in microstructural quality going from Za1 to Za4 directly correlates with the gradual decrease of all measured properties tested in this research, indicating that

microstructural densification is ultimately the chief mechanism responsible for the greater performance of the quaternary nanocomposite system **(Suarez and Rincon 2025)**.

4. CONCLUSIONS

The incorporation of quaternary nanocomposites (nano-chitosan/PVA/PAA/AgNPs) prepared via ultrasonication at 1.0 wt.% of cement into Ordinary Portland Cement mortar yielded the following key findings, as confirmed by one-way ANOVA and Tukey's HSD post-hoc test ($p < 0.001$):

1. Mix Za1 (highest level: PVA = 1.50 g, PAA = 0.75 g) showed the best performance compared to all tested properties with compressive strength and water absorption of, respectively, for 28 days equal to 34.33 ± 0;058 MPa (4.7% increase over control:34.80±0;100MPa), a decrease of31.7% and bulk density of 2259 ± l.Okg/m^3 The fact that all properties decreased progressively from Za1 to Za4 with diminishing nanocomposite concentration confirms the clearly dosage-dependent nature of the system.
2. The full initial and final setting times of all nanocomposite mixtures were also higher than in the control, the longest being 193 and 307 minutes for Za1 (12.9% and 7.7% increases, respectively) which could be favorable to workability under high temperature conditions like Iraq.
3. The results of XRD analysis confirmed the efficient in-situ preparation of AgNPs during ultrasonication and the primarily amorphous nature of the nanocomposites, and SEM imaging demonstrated that Za1 possessed a dense, homogeneous and crack-free microstructure, whereas Za3 had a lamellar or porous structure with air pockets, which directly explained variations in mechanical and physical behavior.
4. The synergistic nucleation mechanism of nano-chitosan in promoting C-S-H gel formation, pore-filling and crack-bridging roles of PVA and PAA, and nano-crosslinking effect of AgNPs make this quaternary nanocomposite system a potential additive for cement mortar applications.

NOMENCALATURE

Symbol	Description	Symbol	Description
A	Cross-sectional area (mm^2)	NC	Nanochitosan
A	mass of oven-dried specimen in air (g)	OPC	Ordinary Portland Cement
AgNPs	Nanoparticals silver nitrate	PAA	Poly acrylic acid
B	mass of surface-dry specimen in air after immersion (g)	PVA	Poly vinyl alcohole
C	apparent mass of specimen suspended in water (g)	SEM	Scanning Electron Microscopy
C-S-H	Calecium silica hydrate	SS	Standard sand
FST	Final setting time (min)	WA	water absorption (%)
IST	Initial setting time (min)	XRD	x-ray diffraction
(ITZ)	Interfacial Transition Zone	ρ	Bulk Density of hardened mortar (kg/m^3)
MO	Control mix	ρw	bulk density of water (1000 kg/m^3)

Credit Authorship Contribution Statement

Zainab Taki Yonuss: Visualization and draft writing, discussion and linguistic review. Sana Hitwer Awad: Conducting and analyzing results, and proofreading.

Declaration of Competing Interest

The authors declare that they have no known competing financial interests or personal relationships that could have appeared to influence the work reported in this paper.

REFERANCES

Abdul Kareem, E. A., Sultan, A. E., and Oraibi, H. M., 2023. Synthesis and characterization of silver nanoparticles: A review. *Ibn AL-Haitham Journal for Pure and Applied Sciences*, 36(3), pp. 177–200. https://doi.org/10.30526/36.3.3050

Abdali, K., Al-Bermany, E., and Abass, K. H., 2023. Impact the silver nanoparticles on properties of new fabricated polyvinyl alcohol-polyacrylamide-polyacrylic acid nanocomposites films. *Journal of Polymer Research*, 30, p. 138. https://doi.org/10.1007/s10965-023-03514-y

Abutu, D., Ameh, A. O., Umunnawuike, C., Barima, M., Nyah, F., Nwaichi, P. I., Charity, O. C., and Yerima, E. A., 2025. Reinforcing concrete with nano-enhanced bio-additives: A path toward sustainable construction materials. *Discover Concrete and Cement*, 1, Article 20. https://doi.org/10.1007/s44416-025-00022-8

Aldakheel, F. M., Mohsen, D., El Sayed, M. M., Alawam, K. A., Binshaya, A. S., and Alduraywish, S. A., 2023. Silver nanoparticles loaded on chitosan-g-PVA hydrogel for wound-healing applications. *Molecules*, 28(7), P. 3241. https://doi.org/10.3390/molecules28073241

AL-Fawares, O., Alshweiat, A., and Al-Khresieh, R. O., 2024. A significant antibiofilm and antimicrobial activity of chitosan-polyacrylic acid nanoparticles against pathogenic bacteria. *Saudi Pharmaceutical Journal*, 32(1), P. 101918. https://doi.org/10.1016/j.jsps.2023.101918

AL sahib, S. A. and Awad, S. H., 2022. Synthesis, characterization of chitosan para-hydroxyl benzaldehyde Schiff base linked maleic anhydride and the evaluation of its antimicrobial activities. *Baghdad Science Journal*, 19(6). https://doi.org/10.21123/bsj.2022.5655

Alwan, Y. T. and Kadhim, F. J., 2025. Optimized characteristics of polyvinyl alcohol films decorated with silver nanoparticles synthesized via chemical reduction method. *Iraqi Journal of Physics*, 23(2), pp. 99–105. https://doi.org/10.30723/ijp.v23i2.1355

ASTM C778, 2017. Standard Specification for Standard Sand. West Conshohocken, PA, USA

ASTM C109/C109M, *2021.* Standard Test Method for Compressive Strength of Hydraulic Cement Mortars (Using 2-in. or [50-mm] Cube Specimens). *West Conshohocken, PA, USA.*

ASTM C191/C191M, *2021.* Standard Test Methods for Time of Setting of Hydraulic Cement by Vicat Needle. *West Conshohocken, PA, USA.*

ASTM C642, *2021.* Standard Test Method for Density, Absorption, and Voids in Hardened Concrete. *West Conshohocken, PA, USA.*

Baykara, H., Riofrio, A., Garcia-Troncoso, N., Cornejo, M., Tello-Ayala, K., Flores Rada, J., and Caceres, J., 2024. Chitosan-cement composite mortars: Exploring interactions, structural evolution,

environmental footprint and mechanical performance. *ACS Omega*, 9(23), pp. 24978–24986. https://doi.org/10.1021/acsomega.4c02040

Chicea, D. and Nicolae-Maranciuc, A., 2024. Silver nanoparticles-chitosan nanocomposites: A comparative study regarding different chemical syntheses procedures and their antibacterial effect. *Materials*, 17(5), P. 1113. https://doi.org/10.3390/ma17051113

Choi, S. J., Bae, S. H., Lee, J. I., Bang, E. J., and Ko, H. M., 2021. Strength, carbonation resistance, and chloride-ion penetrability of cement mortars containing catechol-functionalized chitosan polymer. *Materials*, 14(21), P. 6395. https://doi.org/10.3390/ma14216395

Fang, Y., Wu, C., Hu, S., and Zhou, Y., 2024. Study on the correlation between mechanical properties, water absorption, and bulk density of PVA fiber-reinforced cement matrix composites. *Buildings*, 14(11), P. 3580. https://doi.org/10.3390/buildings14113580

González-Lara, H., Parra-Pacheco, B., Rico-García, E., Aguirre-Becerra, H., Feregrino-Pérez, A. A., and García-Trejo, J. F., 2025. Black soldier fly culture as a source of chitin and chitosan for its potential use in cement mortar: An overview. *Polymers*, 17(6), P. 717. https://doi.org/10.3390/polym17060717

Han, F., Wang, W. R., and Li, D. Y., 2023. Simple synthesis of silver nanocluster composites AgNCs@PE-g-PAA by irradiation method. *Nuclear Science and Techniques*, 34, P. 73. https://doi.org/10.1007/s41365-023-01224-0

IQS No. 5, 2019. Ordinary Portland Cement. Central Organization for Standardization and Quality Control (COSQC), Baghdad, Iraq.

IQS No. 1703, 2018. Water Used for Concrete and Cement Mortar. Central Organization for Standardization and Quality Control (COSQC), Baghdad, Iraq.

Mohamed, R. R., 2018. Green synthesis of antimicrobial and antitumor N,N,N-trimethyl chitosan chloride/poly(acrylic acid)/silver nanocomposites. *International Journal of Biological Macromolecules*. https://doi.org/10.1016/j.ijbiomac.2018.01.055

Paciejewski, M., Lange, A., Jaworski, S., Kutwin, M., Bombalska, A., Siwiński, J., Olkowicz, K., Mierczyk, J., Narojczyk, K., Bogdanowicz, Z., and Nasiłowska, B., 2024. Effect of doping cement mortar with triclosan, hypochlorous acid, silver nanoparticles and graphene oxide on its mechanical and biological properties. *Materials*, 17(24), P. 6288. https://doi.org/10.3390/ma17246288

Pan, Z., Liu, Y., and Zhao, J., 2024. Study on the effect of citric acid-modified chitosan on the mechanical properties, shrinkage properties, and durability of cement mortar. *Materials*, 17(9), P. 2053. https://doi.org/10.3390/ma17092053

Popescu, I., Constantin, M., Pelin, I. M., and Suflet, D. M., 2022. Eco-friendly synthesized PVA/chitosan/oxalic acid nanocomposite hydrogels embedding silver nanoparticles as antibacterial materials. *Gels*, 8(5), P. 268. https://doi.org/10.3390/gels8050268

Rasin, F. A., Abbas, L. K., and Kadhim, M. J., 2017. Study the characterizations of cement mortar by nano pozzolanic materials additions. *Al-Khwarizmi Engineering Journal*, 13(4), pp. 152–163. https://doi.org/10.22153/kej.2017.06.004

Saeed, R. S., Shlaka, W. A., and Negim, E., 2024. Synthesis and study medical application of nanocomposites based on grafted chitosan/polyvinyl alcohol. *Ibn AL-Haitham Journal for Pure and Applied Sciences*, 37(1). https://doi.org/10.30526/37.1.3327

Shareef, A. A., Hassan, Z. A., Kadhim, M. A., and Al-Mussawi, A. A., 2022. Antibacterial activity of silver nanoparticles synthesized by aqueous extract of Carthamus oxycantha against antibiotics resistant bacteria. *Baghdad Science Journal*, 19(3), P. 460. https://doi.org/10.21123/bsj.2022.19.3.0460

Soman, V., Vishwakarma, K., and Poddar, M. K., 2023. Ultrasound assisted synthesis of polymer nanocomposites: A review. *Journal of Polymer Research*, 30, P. 406. https://doi.org/10.1007/s10965-023-03786-4

Suslick, K. S. and Price, G. J., 2010. Applications of ultrasound to the synthesis of nanostructured materials. *Advanced Materials*, 22(10), pp. 1039–1059. https://doi.org/10.1002/adma.200904093

Sybis, M., Staninska-Pięta, J., Piotrowska-Cyplik, A., and Konował, E., 2026. Nanosilver Modified Concrete as a Sustainable Strategy for Enhancing Structural Resilience to Flooding. *Sustainability*, 18(2), P. 945. https://doi.org/10.3390/su18020945

Watanuki Filho, A., Higuti, R. T., de Moura, M. R., and Aouada, F. A., 2022. Synthesis, application and effect of hybrid nanocomposites based on hydrogel and nanoclay in cement-mortars. *Polymers*, 14(21), p. 4564. https://doi.org/10.3390/polym14214564

Yang, D., Liu, Q., Gao, Y., Wan, S., Meng, F., Weng, W., and Zhang, Y., 2023. Characterization of silver nanoparticles loaded chitosan/polyvinyl alcohol antibacterial films for food packaging. *Food Hydrocolloids*, 136, p. 108305. https://doi.org/10.1016/j.foodhyd.2022.108305

Yang, Q., Yang, Q., Pen, X., et al., 2025. A review of the effects of nanomaterials on the properties of concrete. *Buildings*, 15(13), P. 2363. https://doi.org/10.3390/buildings15132363

Yehia, S., Ibrahim, A., and Fathy, D., 2023. The impact of using natural waste biopolymer cement on the properties of traditional/fibrous cement mortar. *Innovative Infrastructure Solutions*, 8, P. 275. https://doi.org/10.1007/s41062-023-01253-z

Yu, L., Fan, Q., Meng, D., Meng, X., and Xu, B., 2025. Application and mechanism study on optimal design of cement-based building materials based on polymer binder. *Buildings*, 15(17), P. 3192. https://doi.org/10.3390/buildings15173192

مركبات نانوية من الكيتوزان /PVA/PAA–Ag مصنعة بالموجات فوق الصوتية لتحسين ملاط السمنت

زينب تقي يونس*، سناء هتور عواد

قسم الكيمياء، كلية العلوم للبنات، جامعة بغداد، بغداد، العراق

الخلاصة

أثبت تعديل البنية المجهرية للمواد الإسمنتية باستخدام تقنية النانو أنه طريقة فعالة لتحسين الخواص الميكانيكية وخواص المتانة للمتراكبات المعتمدة على الإسمنت. إلا أن الدراسات السابقة كانت محدودة بالمواد النانوية المفردة أو الأنظمة الثنائية، كما أن التفاعل بين المتراكبات البوليمرية الحيوية والجسيمات النانوية المعدنية أثناء التحضير باستخدام الموجات فوق الصوتية لم تتم دراسته بشكل كافٍ. في هذه الدراسة تم تخليق متراكب نانوي هجين رباعي يتكون من الكيتوسان النانوي، وبولي فاينيل الكحول (PVA)، وحامض البولي أكريليك(PAA) ، والجسيمات النانوية للفضة(AgNPs) ، وإضافته إلى مونة الإسمنت. لتحضير المتراكب النانوي، تم تثبيت كمية الكيتوسان النانوي وتغيير كميات كل من PVA وPAA، مع تثبيت كمية نترات الفضة ($AgNO_3$)عند (10 مل). وتم تعزيز تشتت الجسيمات النانوية والترابط البيني باستخدام الموجات فوق الصوتية. كانت نسبة المونة (الإسمنت:الرمل) 1:2.75، ونسبة الماء إلى الإسمنت 0.485، وتمت إضافة المتراكب النانوي بنسبة (1.0% وزناً من الإسمنت). تم تحديد مقاومة الانضغاط بعد 7 و28 يوماً وفقاً للمواصفةASTM C109 ، بينما تم إجراء فحص امتصاص الماء وفقASTM C642 ، وتحديد الكثافةالكلية وفق نفس المواصفة. كما تم قياس زمن التصلب الابتدائي وفق ASTM C191. أظهرت النتائج تحسناً ملحوظاً في أداء المونة مقارنة بالمونة المرجعية. إذ ازدادت مقاومة الانضغاط بنسبة وصلت إلى 4.6%، بينما انخفض كل من امتصاص الماء والنفاذية، وتحسنت الكثافة الحجمية. كما لوحظ تحسن طفيف في زمن التصلب الابتدائي مما ساهم في تحسين قابلية التشغيل. وتُعزى هذه التحسينات إلى تأثير التنوية للكيتوسان النانوي، وتكوين شبكة بوليمرية ثلاثية الأبعاد بواسطة PVA وPAA، وتأثير التشابك النانوي الناتج عن جسيمات الفضة النانوية، والتي أدت مجتمعة إلى زيادة كثافة المصفوفة وتحسين الترابط البيني .

الكلمات المفتاحية: مونة السمنت، الكيتوسان النانوي، بولي كحول الفاينيل، بولي اكريلك اسيد، التخليق بالموجات فوق الصوتية